Bone Reports 2 (2015) 44–51

Contents lists available at ScienceDirect

Bone Reports

journal homepage: www.elsevier.com/locate/bonr

Original Full Length Article

Study of DXA-derived lateral–medial cortical bone thickness in assessing hip fracture risk

Yujia Long [a], William D. Leslie [b,c], Yunhua Luo [a,*]

[a] Department of Mechanical Engineering, Faculty of Engineering, University of Manitoba, Winnipeg, MB R3T 2N2, Canada
[b] Department of Radiology, Faculty of Medicine, University of Manitoba, Winnipeg, MB R2H 2A6 Canada
[c] Department of Internal Medicine, Faculty of Medicine, University of Manitoba, Winnipeg, MB R2H 2A6 Canada

ARTICLE INFO

Article history:
Received 24 June 2014
Received in revised form 2 February 2015
Accepted 5 February 2015
Available online 8 April 2015

Edited by Peter Ebeling

Keywords:
Osteoporosis
Hip fracture
Cortical bone thickness
Dual energy X-ray absorptiometry (DXA)
Areal bone mineral density (aBMD)

ABSTRACT

The currently available clinical tools have limited accuracy in predicting hip fracture risk in individuals. We investigated the possibility of using normalized cortical bone thickness (NCBT) estimated from the patient's hip DXA (dual energy X-ray absorptiometry) as an alternative predictor of hip fracture risk. Hip fracture risk index (HFRI) derived from subject-specific DXA-based finite element model was used as a guideline in constructing the mathematical expression of NCBT. We hypothesized that if NCBT has stronger correlations with HFRI than the single risk factors such as areal BMD (aBMD), then NCBT can be a better predictor. The hypothesis was studied using 210 clinical cases, including 60 hip fracture cases, obtained from the Manitoba Bone Mineral Density Database. The results showed that, in general HFRI has much stronger correlations with NCBT than any of the single risk factors; the strongest correlation was observed at the superior side of the narrowest femoral neck with $r^2 = 0.81$ ($p < 0.001$), which is much higher than the correlation with femoral aBMD, $r^2 = 0.50$ ($p < 0.001$). The capability of aBMD, NCBT, and HFRI in discriminating the hip fracture cases from the non-fracture ones, expressed as the area under the curve with 95% confidence interval, AUC (95% CI), is respectively 0.627 (0.593–0.657), 0.714 (0.644–0.784) and 0.839 (0.787–0.892). The short-term repeatability of aBMD, NCBT, and HFRI, measured by the coefficient of variation (CV, %), was found to be in the range of (0.64–1.22), (1.93–3.41), (3.10–4.16), respectively. We thus concluded that NCBT is potentially a better predictor of hip fracture risk.

1. Introduction

Hip fracture has become a common health problem among the elderly, as it has resulted in an increasingly large number of morbidity and mortality, as well as high medical care costs (Cooper et al., 1992; Melton, 1993; Cranney et al., 2005; Ioannidis et al., 2009; Tosteson et al., 2007; Papaioannou et al., 2000; Wiktorowicz et al., 2001; Cummings and Melton, 2002). The number of hip fractures worldwide is estimated to rise from 1.7 million in 1990 to 6.3 million in 2050 (Cranney et al., 2005). In Canada, over 30,000 hip fractures occur each year, mostly in the elderly over the age of 65 (Papadimitropoulos et al., 1997). Clinical studies have shown that the majority of hip fractures occurred at one of the three locations, the femoral neck (37%), the trochanter region (49%) and the femoral shaft (14%) (Michelson et al., 1995). Low-trauma event and osteoporosis have been identified as the two main causes of hip fractures (Greenspan et al., 1998). One typical scenario of low-trauma event is a fall from a standing height that would not cause any severe injury to a healthy individual. Osteoporosis is a bone disease characterized by reduced bone strength and increased bone fragility. Osteoporosis is a so-called 'silent' disease, as it may not have noticeable symptom until the first bone fracture. Therefore, a reliable and accurate tool for diagnosing osteoporosis and for assessing fracture risk is crucial to initialize an appropriate intervention, for example the use of anti-osteoporosis drugs or physical therapies, to improve bone quality and to prevent bone fracture. Areal (or projected) bone mineral density (aBMD) extracted from the subject's hip DXA is presently the gold standard for screening osteoporosis (Kanis et al., 2008). FRAX (Fracture Risk Assessment Tool) is another tool available for predicting 10-year fracture probability (RAX®: WHO Fracture Risk Assessment Tool). The tools have been demonstrated as very valuable in studying the epidemiology of osteoporosis (Kanis et al., 2011; Lewiecki et al., 2011a, 2011b; Leslie et al., 2010). But they have limited accuracy in predicting fracture risk in individual patients (Kanis et al., 2011; Marshall et al., 1996; Stone et al., 2003; Cranney et al., 2007). Finite element analysis (FEA) has been a powerful and popular tool for solving various engineering problems. Finite element analysis of hip fracture based on medical images is a promising tool to improve prediction of fracture risk in individuals (Koivumäki et al., 2012a, 2012b;

* Corresponding author at: E2-327 EITC, 75A Chancellor's Circle Department of Mechanical Engineering University of Manitoba Winnipeg, R3T 5V6 Canada.
E-mail address: Yunhua.Luo@umanitoba.ca (Y. Luo).

http://dx.doi.org/10.1016/j.bonr.2015.02.003

Naylor et al., 2013; Keyak et al., 2001a, 2001b; Luo et al., 2011, 2013; Bessho et al., 2007; MacNeil and Boyd, 2008; Lotz et al., 1991; Dickinson et al., 2010; Rhee et al., 2009; Trabelsi et al., 2011; Orwoll et al., 2009; Cody et al., 1999, 2000; Dall'Ara et al., 2013; Lenaerts and Van Lenthe, 2009; Testi et al., 1999; Christen et al., 2010; Langton et al., 2009; Qian et al., 2009; Den Buijs and Dragomir-Daescu, 2011). Hip fracture is resulted by the applied force exceeding its strength. Therefore, whether or not a hip fracture would occur is jointly determined by a number of factors, including bone mechanical properties, bone geometry and the applied force. These factors have not been properly considered in the current clinical tools. FEA is able to integrate all factors affecting bone fracture based on the well-established mechanical principles and governing equations. However, FEA has not been adopted into routine clinical procedure mainly due to its technical complexities. A lengthy training is usually required for a clinician to effectively use FEA software. The objective of this study is to develop a reliable hip fracture risk predictor that has the same or similar accuracy as FEA, but can be easily implemented and adopted into clinic.

2. Materials and methods

The femur bone is composed of two compartments, the cortical bone and the trabecular bone, with cortical bone making up more than 80% of the mass (Jee, 2001). The cortical bone determines the strength of the femur bone and thus its fracture risk. The cortical bone withstands much greater load than the trabecular bone (Bayraktar et al., 2004), and it is the main part in resisting axial force. In addition, the cortical bone is formed as a shell around the trabecular bone. This structural arrangement also makes the cortical bone bear the major portion of bending moment acting on the femur. Therefore, it is rational to develop a risk predictor based on cortical bone quality in the femur. Femur bone strength can be evaluated by its cortical thickness together with the bone mineral density, as the two parameters determine the axial and the bending resistant capacity of the femur. However, the thickness of femur cortical bone is not uniform along either the longitudinal or the circumferential direction; it is best measured by a three-dimensional imaging modality, for example, the quantitative computed tomography (QCT) (Johannesdottir et al., 2014). Unfortunately, QCT has not been adopted into the routine clinical procedure due to its high cost and radiation dose. In the following, we will develop a method to estimate cortical bone thickness based on DXA image. As DXA is routinely used in osteoporosis screening and monitoring, the developed method would have wider applications in clinic if it is successful. The challenge is that the mineral density information captured in a DXA image is an amalgam of contributions from both of the trabecular and the cortical bone, projected along the X-ray direction. The very first question would be: is it possible to measure cortical bone thickness from a single-view DXA image? Fortunately, a useful feature observed from the projected bone density profile provided a solution. The feature was observed with the aid of the QCT Pro software, a medical image processing tool developed by Mindways Software Inc., Austin, USA. QCT Pro can project three-dimensional QCT scans into CTXA, a two-dimensional image that is equivalent to clinical DXA (Khoo et al., 2009). The useful feature is illustrated in Fig. 1 by a typical clinical case obtained from the Great-West Life PET/CT Center, Winnipeg, Canada.

Fig. 1(a) shows the CTXA generated from the clinical QCT scans by the QCT Pro software. Consider the three critical cross-sections at, respectively, the narrowest femoral neck (AB), the intertrochanter (CD) and the femoral shaft (EF), the femur cross-sections and the corresponding aBMD profiles are plotted in Fig. 1(b), (c) and (d). The femur cross-sections were dissected from the QCT scans using the QCT Pro software; the aBMD profiles were generated from the CTXA image using in-house developed MATLAB codes. It can be observed from the aBMD profiles, for each cross-section there exist two distinct peaks,

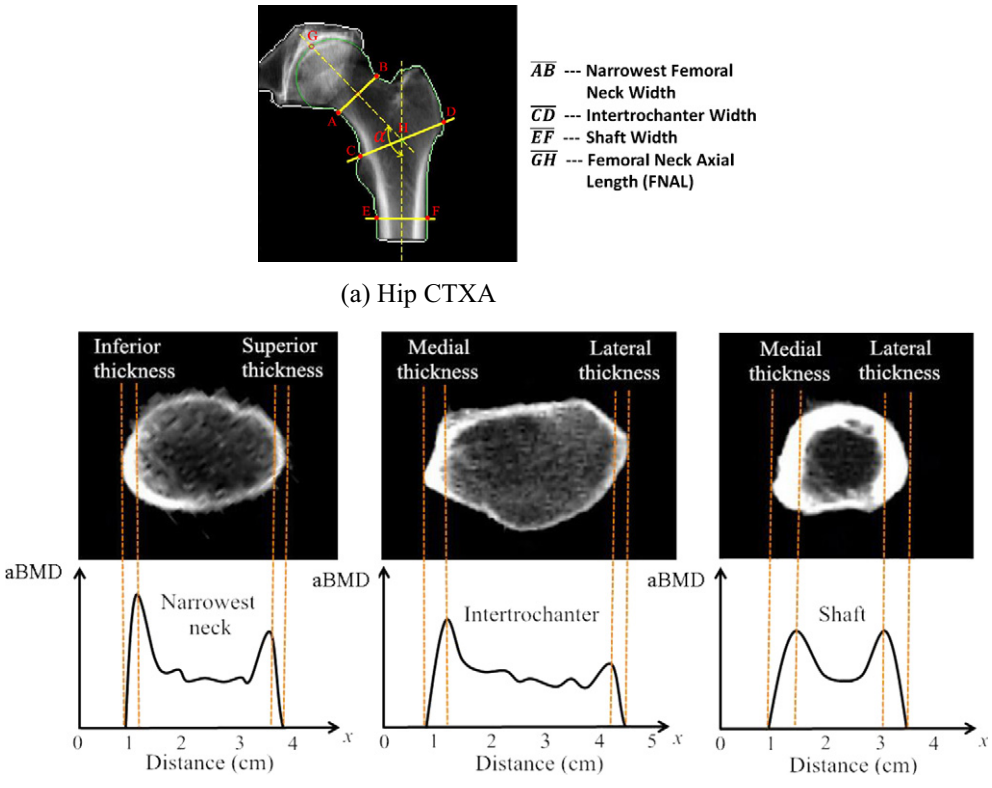

(a) Hip CTXA

(b) Narrowest femoral neck (AB) (c) Intertrochanter (CD) (d) Femoral shaft (EF)

Fig. 1. (a) Hip CTXA projected from QCT scans by QCT Pro; Femur cross-section and the corresponding aBMD profile at (b) the femoral neck (AB), (c) the intertrochanter (CD), and (d) the femoral shaft (EF).

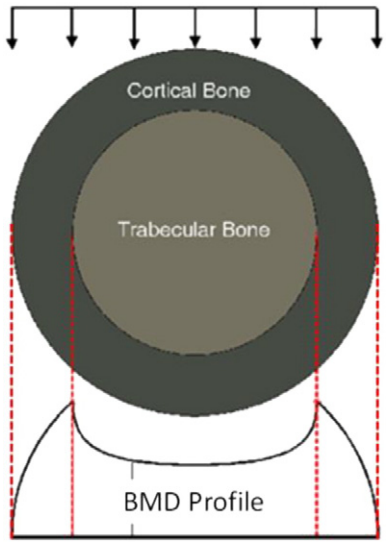

Fig. 2. Projection of circular composite cross-section of two densities.

each at the medial (inferior) and the lateral (superior) side respectively; the peaks are exactly located at the projection line of the inner surfaces of the cortical bone. These peaks can be easily identified as they are usually much higher than their neighbors. The thicknesses of the cortical bone at the medial and the lateral side can be determined by using the two peaks, the starting point and the ending point of the aBMD profile, as illustrated in Fig. 1(b), (c) and (d).

The above observed feature is not a coincidence. It is a common feature in the projection of any round composite cross-section with two densities. The feature can be easily verified by projecting the composite circular cross-section in Fig. 2 and then obtaining its aBMD profile. For simplicity, the cortical bone and the trabecular bone have been assigned constant densities. The aBMD profile can be easily obtained by calculating the lengths of the projection lines through the cross-section and then multiplying them by the corresponding density. The obtained aBMD profile is shown at the bottom of Fig. 2.

There also exist two distinct peaks in the aBMD profile as shown in Fig. 2, but their shapes are not as smooth and round as those in Fig. 1. The reason is that there is a jump between the densities in the composite cross-section, while the transition between cortical and trabecular compartment in real bone is gradual and smoother.

Based on the above feature, we developed an algorithm to determine femur cortical bone thicknesses from clinical hip DXA. The algorithm was implemented in MATLAB codes. The MATLAB codes mainly have the following functions: 1) to automatically locate the three cross-sections (as shown in Fig. 1) based on provided location definitions; 2) to extract aBMD profiles over the three cross-sections; 3) for each of the aBMD profiles, to automatically identify the two distinct peaks; and 4) to determine the cortical bone thicknesses on the medial and the lateral side of the three cross-sections. The algorithm was validated using the Bone Investigation Toolkit (BIT) included in the QCT Pro software. Femur QCT scans of 40 patients were obtained from the Great-West Life PET/CT Center located at Winnipeg, Canada. For each patient, the QCT scans were projected into a CTXA image; then, the cortical bone thicknesses were determined using the MATLAB codes. The above obtained thicknesses were compared with those determined by the BIT software. In the BIT software, femur cortical thickness is determined by the following steps. First, a threshold is selected to separate the cortical bone and the trabecular bone. In our study, a threshold of 450 mg/cm^3 was used based on the suggestions provided in the BIT users' manual and in the literature (MacNeil and Boyd, 2008); then, the cross-section is equally divided into eight sectors (see Fig. 3). For each sector an average thickness is determined. A sample BIT analysis report is provided in Fig. 4, where cortical bone thicknesses of the eight sectors at the intertrochanteric cross-section are listed. If the patient is properly positioned by following the clinical guidelines, Sector 3 in Fig. 3 roughly corresponds to the lateral/superior side, while Sector 7 approximately relates to the medial/inferior side of the femur.

Limited by the two-dimensional feature of CTXA or DXA image, cortical thickness can only be estimated at the medial side and the lateral side. However, the lateral/medial cortical thicknesses are useful in evaluating hip fracture risk. Sideways (or lateral) fall has been identified as the most critical situation for old people to develop hip fracture (Nankaku et al., 2005; Silva, 2007), as the hip is covered with very little soft tissue. In a sideways fall, the bending loading is applied in the coronal plane; therefore, a crack is usually initiated from either the medial or the lateral side of the femur. A thicker cortical bone at the locations would provide larger resistance to crack initiation. However, cortical bone thickness alone cannot predict hip fracture accurately, as hip fracture is also affected by other factors, for example, the geometric and physical parameters of the human body. A number of hip fracture risk factors have been identified in the previous studies (Johannesdottir et al., 2014; Karlamangla et al., 2004; Emaus et al., 2014; Augat et al., 1996; Michelotti and Clark, 1999). From the mechanical point of view, they mainly include the cortical bone thickness (CBT), aBMD, femoral neck axial length (FNAL), neck-shaft angle (α), body weight and height, or body mass index (BMI). We studied how these risk factors affect hip fracture using the subject-specific DXA-based finite element analysis (FEA) (Luo et al., 2011, 2013). The procedure of DXA-based FEA is illustrated in Fig. 5 and briefly described in the following. For more detailed information, the readers are referred to references (Luo et al., 2011, 2013).

The procedure starts with a hip DXA of the concerned patient. The proximal femur is segmented from the DXA and used in generation of the finite element mesh. Bone mechanical properties are assigned to the finite element model using empirical functions that relate bone elasticity modulus and yield stress to bone areal BMD (Den Buijs and

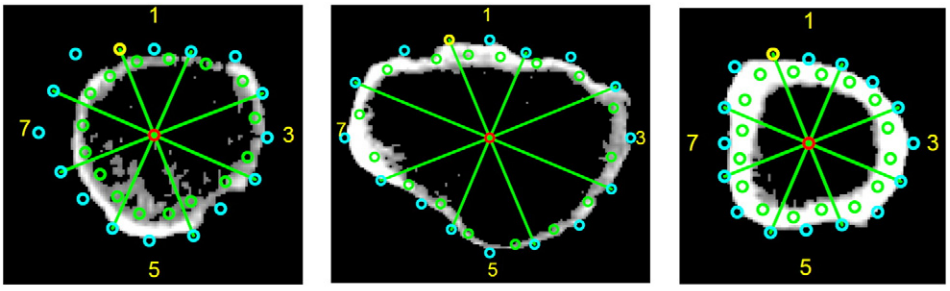

Fig. 3. Determining cortical bone thicknesses using BIT. (a) narrowest femoral neck; (b) intertrochanter; (c) femoral shaft.

	Perimeter	BMD	Area	Cortical Width	Norm Width	Avg Cort Arc Length	Cortical Perimeter	Distance To CM	Distance To Center	Tangent Angle	Curvature	Radius of Curvature
Sector	(cm)	(mg/cm^3)	(cm^2)	(mm)	(mm)	(mm)	(mm)	(mm)	(mm)	(degrees)	(cm^{-1})	(cm)
1	1.96	700.5	0.827	5.28	4.52	15.68	18.14	16.79	19.27	178.5	0.204	4.89
2	2.57	628.1	0.663	3.14	2.41	21.15	22.58	23.33	22.40	-16.0	0.319	3.14
3	2.94	486.4	1.054	4.17	2.48	25.38	27.00	32.40	28.89	-72.9	0.460	2.17
4	2.40	474.2	0.527	2.48	1.45	21.25	22.11	30.55	26.22	-132.6	0.345	2.90
5	2.35	441.5	0.284	1.41	0.78	20.74	21.28	26.70	23.90	-176.7	0.448	2.23
6	2.19	542.2	0.536	2.95	1.97	18.12	19.45	20.14	20.51	144.3	0.049	20.57
7	2.94	807.8	1.354	5.39	5.33	25.07	27.78	25.34	28.69	122.4	0.586	1.71
8	3.14	702.0	0.935	3.79	3.22	25.36	27.62	20.69	24.96	39.7	0.333	3.00
Sum	20.49	4782.6	6.180	28.60	22.17	172.75	185.97	195.95	194.85	86.8	2.745	40.61
Average	2.56	597.8	0.772	3.57	2.77	21.59	23.25	24.49	24.36	10.8	0.343	5.08
Std Dev	0.41	131.8	0.341	1.37	1.53	3.56	3.78	5.33	3.54	132.4	0.165	6.33

Fig. 4. Sample BIT analysis report of the intertrochanteric cross-section in Fig. 3(b).

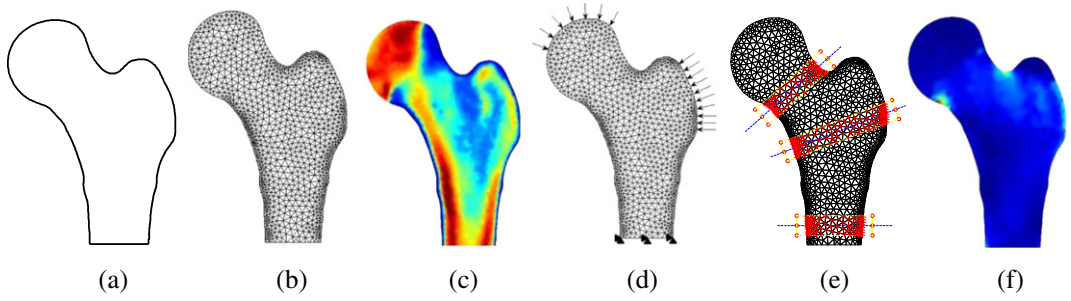

Fig. 5. The procedure of subject-specific DXA-based FEA. (a) Femur contour segmented from the patient's hip DXA; (b) a finite element mesh generated from the contour; (c) assignment of material properties; (d) application of loading/boundary conditions; (e) the three regions of interest (ROI) for assessing hip fracture risk; (f) fracture risk distribution.

Dragomir-Daescu, 2011). Loading and constraint conditions simulating a sideways fall are applied to the finite element model. Stress fields over the femur are obtained by finite element analysis. Fracture risk indices (η_{ROI}) over the three regions of interest (ROI) are calculated based on the definition given in Eq. (1)

$$\eta_{ROI} = \frac{\sum_{i=1}^{N} \int_{A_i} \frac{\sigma_{eff}}{\sigma_Y} dA}{\sum_{i=1}^{N} A_i}. \quad (1)$$

In the above equation, η_{ROI} is the fracture risk index over an ROI, for example, the femoral neck, intertrochanteric region, proximal shaft, as shown in Fig. 5(e). A_i ($i = 1, 2, \ldots, N$) are the areas of the finite elements encompassed in the ROI. σ_{eff} and σ_Y are, respectively, the von Mises stress and the yield stress at the Gaussian points in element *i*. Bone yield stress has been used as a failure criterion as the human proximal femur behaves linearly elastic up to failure under physiological loading conditions (Juszczyk et al., 2011). Although bone is a typical anisotropic material, DXA is inherently two-dimensional and the information required for constructing anisotropic finite element model is not available from DXA. However, Buijs et al. (Den Buijs and Dragomir-Daescu, 2011) have demonstrated that bone strengths predicted by DXA-based FE model have good correlation with experiment results.

To investigate the possibility and effectiveness of using femur cortical bone thickness (CBT) as a predictor of hip fracture risk, 210 clinical cases were acquired from the Manitoba Bone Mineral Density Database in an anonymous way under a human research ethics approval. All the subjects were scanned using Lunar Prodigy DXA scanner with a standard mode (37.0 μGy). Each DXA image was converted and saved in a MATLAB mat-file. For each case, the acquired information includes a DXA image, the subject's age, body height, weight, and aBMD over the ROIs. The statistics of the clinical cases are provided in Table 1. The clinical cases consist of 60 hip fracture cases and 150 non-fracture ones. In 30 of the non-fracture cases, each has an initial and a repeat DXA that were scanned from the same subject within several days; In these cases one should expect no change in the fracture risk.

Table 1
Statistics of 210 clinical cases.

Parameters	Mean (SD)	
	60 cases	150 controls
Age (years)	69.2 (3.5)	65.4 (9.3)
Height (in.)	63.1 (2.3)	62.7 (2.2)
Weight (lbs.)	129.4 (29.7)	144.8 (31.4)
Femoral neck aBMD (g/cm^2)	0.712 (0.059)	0.806 (0.147)
Trochanteric aBMD (g/cm^2)	0.576 (0.068)	0.669 (0.168)
Total hip aBMD (g/cm^2)	0.738 (0.066)	0.843 (0.179)

Table 2
Average relative error (*e*, %) between CTXA and QCT-derived cortical bone thickness.

Femoral neck		Intertrochanter		Shaft		All six locations
Inferior	Superior	Medial	Lateral	Medial	Lateral	
5.76	7.95	6.18	8.13	5.03	5.74	6.51

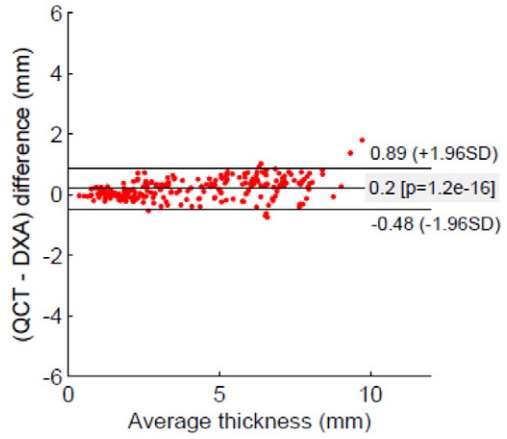

Fig. 6. Bland–Altman plot of QCT and DXA measured cortical bone thicknesses.

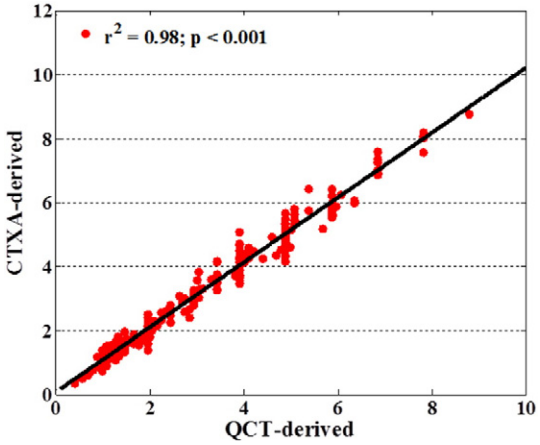

Fig. 7. Correlation between CTXA and QCT-derived cortical bone thicknesses.

Correlations between HFRI and the fracture risk factors were first studied. For each case, a finite element model was constructed by the previously described procedure. Fracture risk indices were calculated. Femur geometric parameters such as the narrowest femoral neck width and the femoral neck axial length were extracted from the DXA images using in-house developed MATLAB codes. Correlations between HFRI and the risk factors were then investigated using SPSS software (IBM SPSS 22, New York, USA). From the results we found that among all the factors, HFRI has the strongest correlation with CBT; HFRI is positively correlated to the neck-shaft angle (α), the cortical bone thickness (CBT) and the areal bone mineral density (aBMD), and negatively correlated to the femoral neck axial length (FNAL) and body mass index (BMI). These findings suggested that an effective predictor of hip fracture should be constructed with CBT as the main player. Therefore, we

Table 4
Correlations between hip fracture risk index (HFRI) and normalized cortical bone thickness (NCBT), (r^2, p-value).

Femoral neck	Inferior	−0.63[a] (<0.001)
	Superior	−0.81 (<0.001)
Intertrochanter	Medial	−0.70 (<0.001)
	Lateral	−0.75 (<0.001)
Femur shaft	Medial	−0.60 (<0.001)
	Lateral	−0.67 (<0.001)

[a] A negative sign indicates a negative correlation.

proposed the following normalized cortical bone thickness (NCBT) as a new predictor of hip fracture risk

$$\mathrm{NCBT} = \frac{\mathrm{CBT} \times \mathrm{aBMD}}{\alpha \times \mathrm{FNAL} \times \mathrm{BMI}}. \quad (2)$$

It should be noted that NCBT is a dimensionless parameter. The numerator is the product of cortical thickness and areal BMD, approximately representing the strength of the cortical bone at the concerned location. The denominator is a combination of the femur geometry and the body anthropometry, roughly representing the femoral geometry and the loading condition in a sideways fall. It is hypothesized that if a stronger correlation exists between HFRI and NCBT than any of the single risk factors, NCBT can be used as a better predictor of hip fracture risk.

The overall discriminative values of aBMD, CBT and HFRI for hip fracture, measured by the area under the Receiver Operating Characteristic (ROC) curve (AUC) with 95% of confidence interval (95% CI) (Trémollieres et al., 2010), were also calculated using SPSS. The short-term repeatability of aBMD, CBT and HFRI, measured by the coefficient of variation (CV, %) (Luo et al., 2013; Gluer et al., 1995), were studied using the 30 pairs of clinical DXA.

3. Results

The difference between CTXA and QCT derived cortical thickness is measured by the following relative error

$$e = \frac{|t_{CTXA} - t_{QCT}|}{t_{QCT}} \quad (3)$$

where t_{CTXA} and t_{QCT} denote, respectively, CTXA and QCT derived cortical thickness. The average relative errors are listed in Table 2. Bland–Altman plot of CTXA and QCT measured cortical thicknesses is displayed in Fig. 6. Correlation between the CTXA and QCT derived CBT is displayed in Fig. 7. Correlations between HFRI and single risk factors are presented in Table 3, where a negative sign indicates a negative correlation. Correlations between HFRI and NCBT at the medial side and lateral side of the three critical cross-sections are provided in Table 4. The overall discriminative values of aBMD, NCBT and HFRI, expressed as AUC (95% CI), are presented in Table 5. Mean values of aBMD, CBT, NCBT and HFRI in the cases and controls are listed in Table 6. The relative difference in the table is defined as the ratio of the difference

Table 3
Correlations between HFRI and risk factors (r^2, p-value).

Fracture risk factors	Cortical bone thickness		Areal BMD	Body mass index (BMI)	Femoral neck axial length (FNAL)	Neck-shaft angle (α)
	Medial/inferior	Lateral/superior				
Femoral Neck	−0.39[a] (<0.001)	−0.68 (<0.001)	−0.50 (<0.001)	0.32 (<0.001)	0.37 (<0.001)	0.34 (<0.001)
Intertrochanter	−0.36 (<0.001)	−0.60 (<0.001)	−0.43 (<0.001)	0.27 (<0.001)	0.35 (<0.001)	0.28 (<0.001)
Femoral shaft	−0.35 (<0.001)	−0.57 (<0.001)	−0.22 (<0.001)	0.25 (<0.001)	0.33 (<0.001)	0.31 (<0.001)

[a] A negative sign indicates a negative correlation.

Table 5
AUC (95% CI) of aBMD, NCBT and HFRI.

Hip fracture risk indicator		AUC	95% CI
Femoral neck BMD		0.625	0.593–0.657
HFRI (at femoral neck) derived from DXA-based FE model		0.839	0.787–0.892
NCBT at femoral neck	Superior	0.714	0.644–0.784
	Inferior	0.706	0.634–0.778

Table 6
Fracture risk indicators in cases and controls [Mean (SD)].

Fracture risk indicator		60 cases	150 controls	Relative difference (%)
	aBMD	0.712 (0.084)	0.806 (0.147)	12.4
CBT	Superior (mm)	1.881 (0.292)	2.133 (0.373)	12.6
	Inferior (mm)	3.193 (0.544)	3.410 (0.581)	6.6
NCBT	Superior (10^{-3})	0.340 (0.079)	0.433 (0.135)	24.1
	Inferior (10^{-3})	0.573 (0.122)	0.687 (0.204)	18.1
	HFRI	1.628 (0.357)	1.054 (0.456)	42.8

between the means (of the cases and the controls) to their average. The relative difference indicates the overall ability of the parameters in distinguishing cases from controls. Short-term variations of aBMD, NCBT and HFRI measured by CV (%) are given in Tables 7, 8 and 9.

4. Discussions

The relative errors shown in Table 2 and Fig. 6 are in an acceptable scope but not trivial. Differences between the CTXA and QCT derived thicknesses may have been introduced from a number of sources in the described method. The segmentation thresholds used in separating the proximal femur from the surroundings in both CTXA and QCT may have introduced nontrivial differences. The selection of a proper segmentation threshold depends on a number of factors, for example, scanner settings and noises, which may introduce either systematic or random errors. The use of a slightly different threshold in the CTXA segmentation would shift the contour of the femur, which would change the locations of the starting point and ending point of the three cross-sections, see Fig. 1(a), and thus affect the cortical bone thicknesses. Similarly, a different segmentation threshold selected in the BIT toolkit may have affected the cortical bone thicknesses derived from QCT. In addition, the CBTs determined by the BIT software are average thicknesses of the eight sectors, while the CBTs determined from CTXA are the thicknesses along the radiant ray in the medial–lateral direction. As the cortical thickness is not uniform along the circumferential direction, theoretically there exists a certain difference between them. However, the strong correlation [$r^2 = 0.98$ ($p < 0.001$)] shown in Fig. 7 and the Bland–Altman plot in Fig. 6 indicate that the differences between the CTXA and QCT derived thicknesses are dominated by systematic or procedural errors, which can be partially corrected by calibration.

As hip fracture risk indicators, one fundamental difference between aBMD and HFRI is that, HFRI is a compound indicator that has integrated effects from all the single indicators including aBMD. Therefore, to investigate the effectiveness of the proposed NCBT in predicting hip fracture, hip fracture risk measurements derived from subject-specific DXA-based finite element models have been used as a baseline for comparison. Extensive researches reported in the literature, for example references (Koivumäki et al., 2012a, 2012b; Naylor et al., 2013; Keyak et al., 2001a, 2001b; Luo et al., 2011, 2013; Bessho et al., 2007; MacNeil and Boyd, 2008; Lotz et al., 1991; Dickinson et al., 2010; Rhee et al., 2009; Trabelsi et al., 2011; Orwoll et al., 2009; Cody et al., 1999, 2000; Dall'Ara et al., 2013; Lenaerts and Van Lenthe, 2009; Testi et al., 1999; Christen et al., 2010; Langton et al., 2009; Qian et al., 2009; Den Buijs and Dragomir-Daescu, 2011) among many others, have demonstrated that subject-specific finite element modeling can better predict hip fracture risk than aBMD. By their independent research work, Langton et al. (2009), Dall'Ara et al. (2013) and Koivumäki et al. (2012a) have reported that femur fracture loads predicted by subject-specific QCT-based finite element models are closely correlated with in-vitro experimental results, with a coefficient of determination $r^2 > 80\%$ ($p < 0.001$), which is much higher than volumetric BMD, $r^2 = 54.5\%$. Although DXA-based finite element models (Luo et al., 2011, 2013; Testi et al., 1999; Den Buijs and Dragomir-Daescu, 2011) are inherently two-dimensional, femur stiffness and strengths predicted by the models are also correlated with experimental data much better than aBMD alone (Den Buijs and Dragomir-Daescu, 2011). That subject-specific finite element modeling is able to more accurately predict fracture risk has its theoretical base. Bone fracture occurs only if the applied load exceeds the strength of the bone. Hip fracture is jointly governed by a number of factors including the subject's body weight/height, bone quality and bone geometry. BMD only represents bone quality. The other factors are missing from the BMD-based fracture risk assessment methods. This explains why BMD alone cannot predict fracture risk accurately. Finite element modeling is able to consider all the mechanical factors affecting hip fracture based on the well-established mechanical equations. Therefore, HFRI derived from DXA-based FE model has much higher accuracy in discriminating clinic hip fractures than BMD alone, as demonstrated by the results in Tables 5 and 6. However, the accuracy and effectiveness of finite element modeling in assessing individual hip fracture risk are closely related to the implementation, especially how the fracture risk is defined. In the DXA-based finite element (FE) model implemented by Naylor et al. (2013), hip fracture risk is measured by the load-strength ratio (LSR); it is a global risk measurement defined over the whole proximal femur. The clinical study results showed that the discriminative capacity of LSR for hip fracture (AUC = 0.69, 95% CI = 0.64–0.73) was only slightly higher than that of femoral BMD (AUC = 0.66, 95% CI = 0.62–0.71). In our DXA-based FE model, fracture risk was measured by local hip fracture risk indices (HFRI) defined over the three regions of interest (ROI), where the majority of hip fractures have been observed in clinic (Michelson et al., 1995). The discriminative capacity of local HFRI has been considerably improved (AUC = 0.839, 95% CI = 0.787–0.892). The local HFRI is able to eliminate adverse effects from the overlap between the pelvis and the femoral head in the DXA image, the stress concentration at the location where constraints are applied, etc.

The correlations between HFRI and the single risk factors (see Table 3) were used as a base in constructing the expression of NCBT in Eq. (2). A larger NCBT or a lower HFRI represents a lower hip fracture

Table 8
Short-term repeatability (CV, %) of NCBT.

Narrowest femoral neck		Intertrochanter		Femoral shaft	
Medial	Lateral	Medial	Lateral	Medial	Lateral
3.27	3.41	2.59	2.85	1.93	2.38

Table 7
Short-term repeatability (CV, %) of areal BMD.

Femoral neck	Trochanteric region	Proximal femur
1.22	0.85	0.64

Table 9
Short-term repeatability (CV, %) of HFRI.

Femoral neck	Intertrochanteric	Femoral shaft
3.10	3.94	4.16

Table 10
Correlations between femoral neck axis length (FNAL) and femur width (r^2, p-value).

	Femoral neck width	Intertrochanteric width	Subtrochanteric width
Femoral neck axis length	0.32 (<0.001)	0.14 (<0.001)	0.17 (<0.001)

risk. Therefore, all the factors having negative correlation with HFRI are put in the numerator of Eq. (2), while the rest of the factors are in the denominator. The obtained results also confirmed our hypothesis, if NCBT has a stronger correlation with HFRI than aBMD, NCBT is a better indicator of hip fracture risk. The AUC values in Table 5 and the mean values in Table 6 showed that HFRI has the highest accuracy in discriminating hip fracture, followed by NCBT and then aBMD. By comparing the correlations in Table 4 with those in Table 3, it can be found that in general NCBT has a much stronger correlation with the HFRI than any of the single risk factors including aBMD. The highest correlation occurred at the superior side of the narrowest femoral neck, probably due to the special loading condition and the small CBT there, with a determination coefficient of $r^2 = 0.81$ ($p < 0.001$), which is much higher than aBMD, $r^2 = 0.50$ ($p < 0.001$). NCBT is also a compound predictor, but it only considers the effects of single risk factors in an approximate way based on the correlations revealed by DXA-based finite element simulations. This explains why in discriminating clinical fracture cases (see Tables 5 and 6), HFRI performed the best, followed by NCBT and then aBMD. In the definition of NCBT, see Eq. (2), the product of CBT and aBMD represents the bone quality; BMI approximately characterizes the loading conditions in a lateral fall (Karlamangla et al., 2004); the femoral neck axial length (FNAL) and the neck-shaft angle (α) are related to the femur geometry. Although the femur width may also be considered as a risk factor, results from the correlation studies (see Table 10) showed that femur widths at the three cross-sections are positively correlated to FNAL. Therefore, the effect of femur width on hip fracture risk has been partially represented by FNAL.

The results in Tables 7, 8 and 9 show that aBMD has the best short-term repeatability, followed by NCBT and then HFRI, they are in a reversed order of their discriminative capacity. As a general rule, a compound parameter usually has lower short-term repeatability than those of the single factors involved. As can be seen from the definition of NCBT in Eq. (2), the short-term repeatability of NCBT is affected by those of the cortical bone thickness (CBT), areal BMD (aBMD), neck-shaft angle (α), femoral neck axial length (FNAL), and body mass index (BMI). In the DXA-based FE modeling, even more factors are involved beside those in the NCBT, for example bone mass distribution and finite element mesh density. Therefore, HFRI derived from DXA-based FE model has an even lower short-term repeatability. If both discriminative capacity and short-term repeatability are taken into consideration, NBCT may be an ideal predictor for hip fracture risk.

NCBT can be conveniently integrated into the current clinical procedure with the existing infrastructures in osteoporosis clinic. Among the five parameters required for calculating NCBT, the aBMD and the BMI are already available from the current DXA report; the neck-shaft angle, the CBT and the FNAL can be easily measured from the patient's hip DXA by the computer codes developed in this study.

5. Conclusion

With a clinical hip DXA (scanned in the anterior–posterior direction), femur CBT can be estimated from the aBMD profile of the concerned cross-section at the medial (inferior) side and the lateral (superior) side. The accuracy of DXA-derived CBT has been validated by the BIT toolkit included in the QCT Pro software. The validation results showed that there indeed exist some non-trivial differences between the QCT and the DXA-derived CBT. However, the differences are dominated by procedural errors, and thus can be reduced by a calibration procedure. Based on correlations revealed by subject-specific DXA-based FE simulations, a more effective risk predictor, NCBT, has been proposed. Study results using clinical cases showed that NCBT has better discriminative capacity of hip fracture than aBMD, and better short-term repeatability than HFRI. It can be easily adopted into a clinical environment. Therefore, it may be an ideal predictor of hip fracture risk.

Acknowledgments

We gratefully acknowledge the funding granted by the Natural Sciences and Engineering Research Council (NSERC) 37098 and the Manitoba Health Research Council (MHRC), Canada, in supporting the reported research work. Thanks are also directed to Ms. Linda Ward at the St. Boniface General Hospital for providing the clinical DXA images and to Dr. Andrew Goertzen at the PET/CT Centre, Winnipeg, for providing the QCT scans.

References

Augat, P., Reeb, H., Claes, L.E., 1996. Prediction of fracture load at different skeletal sites by geometric properties of the cortical shell. J. Bone Miner. Res. 11, 1356–1363.
Bayraktar, H.H., Morgan, E.F., Niebur, G.L., Morris, G.E., Wong, E.K., Keaveny, T.M., 2004. Comparison of the elastic and yield properties of human femoral trabecular and cortical bone tissue. J. Biomech. 37, 27–35.
Bessho, M., Ohnishi, I., et al., 2007. Prediction of strength and strain of the proximal femur by a CT-based finite element method. J. Biomech. 40, 1745–1753.
Christen, D., Webster, D.J., Muller, R., 2010. Multiscale modelling and nonlinear finite element analysis as clinical tools for the assessment of fracture risk. Philos. Transact. A Math. Phys. Eng. Sci. 368, 2653–2668.
Cody, D.D., Gross, G.J., Hou, F.J., et al., 1999. Femoral strength is better predicted by finite element models than QCT and DXA. J. Biomech. 32, 1013–1020.
Cody, D.D., Hou, F.J., Divine, G.W., et al., 2000. Short term in vivo precision of proximal femoral finite element modeling. Ann. Biomed. Eng. 28, 408–414.
Cooper, C., Campion, G., Melton III, L.J., 1992. Hip fractures in the elderly: a world-wide projection. Osteoporos. Int. 2, 285–289.
Cranney, A., Coyle, D., Hopman, W.M., Hum, V., Power, B., Tugwell, P.S., 2005. Prospective evaluation of preferences and quality of life in women with hip fractures. J. Rheumatol. 32, 2393–2399.
Cranney, A., Jamal, S.A., Tsang, J.F., Josse, G.R., Leslie, W.D., 2007. Low bone mineral density and fracture burden in postmenopausal women. CMAJ 177, 575–580.
Cummings, S.R., Melton III, L.J., 2002. Epidemiology and outcomes of osteoporotic fractures. 359, 1761–1767.
Dall'Ara, E., Luisier, B., Schmidt, R., Kainberger, F., Zysset, P., Pahr, D., 2013. A nonlinear QCT-based finite element model validation study for the human femur tested in two configurations in vitro. Bone 52, 27–38.
Den Buijs, J.O., Dragomir-Daescu, D., 2011. Validated finite element models of the proximal femur using two-dimensional projected geometry and bone density. Comput. Methods Prog. Biomed. 104, 168–174.
Dickinson, A.S., Taylor, A.C., Ozturk, H., Browne, M., 2010. Experimental validation of a finite element model of the proximal femur using digital image correlation and a composite bone model. J. Biomech. Eng. 133.
Emaus, N., Wilsgaard, T., Ahmed, L.A., 2014. Impacts of body mass index, physical activity, and smoking on femoral bone loss. The Tromsø Study. J. Bone Miner. Res. http://dx.doi.org/10.1002/jbmr.2232 [Epub ahead of print].
Gluer, C.C., Blake, G., Lu, Y., Blunt, B.A., Jergas, M., Genant, H.K., 1995. Accurate assessment of precision errors: how to measure the reproducibility of bone densitometry techniques. Osteoporos. Int. 5, 262–270.
Greenspan, S.L., Myers, E.R., Kiel, D.P., Parker, R.A., Hayes, W.C., Resnick, N.M., 1998. Fall direction, bone mineral density, and function: risk factors for hip fracture in frail nursing home elderly. Am. J. Med. 104, 539–545.
Ioannidis, G., Papaioannou, A., Hopman, W.M., et al., 2009. Relation between fractures and mortality: results from the Canadian Multicentre Osteoporosis study. Can. Med. Assoc. J. 265–71.
Jee, W., 2001. Integrated bone tissue physiology: anatomy and physiology. In: Cowin, S.C. (Ed.), Bone Mechanics Handbook, 2nd edition CRC Press, New York.
Johannesdottir, F., Turmezei, T., Poole, K.E., 2014. Cortical bone assessed with clinical computed tomography at the proximal femur. J. Bone Miner. Res. 29, 771–783.
Juszczyk, M.M., Cristofolini, L., Viceconti, M., 2011. The human proximal femur behaves linearly elastic up to failure under physiological loading conditions. J. Biomech. 44, 2259–2266.
Kanis, J.A., McCloskey, E.V., Johansson, H., Oden, A., Melton, L.J.I.I.I., Khaltaev, N., 2008. A reference standard for the description of osteoporosis. Bone 42, 467–475.
Kanis, J.A., Hans, D., Cooper, C., et al., 2011. Interpretation and use of FRAX in clinical practice. Osteoporos. Int. 22, 2395–2411.
Karlamangla, A.S., Barrett-Connor, E., Young, J., Greendale, G.A., 2004. Hip fracture risk assessment using composite indices of femoral neck strength: the Rancho Bernardo study. Osteoporos. Int. 15, 62–70.

Keyak, J.H., Rossi, S.A., Jones, K.A., Les, C.M., Skinner, H.B., 2001a. Prediction of fracture location in the proximal femur using finite element models. Med. Eng. Phys. 23 (9), 657–664.
Keyak, J.H., Skinner, H.B., Fleming, J.A., 2001b. Effect of force direction on femoral fracture load for two types of loading conditions. J. Orthop. Res. 19 (4), 539–544.
Khoo, B.C., Brown, K., Cann, C., et al., 2009. Comparison of QCT-derived and DXA-derived areal bone mineral density and T scores. Osteoporos. Int. 20, 1539–1545.
Koivumäki, J.E., Thevenot, J., Pulkkinen, P., Kuhn, V., Link, T.M., Eckstein, F., Jämsä, T., 2012a. Ct-based finite element models can be used to estimate experimentally measured failure loads in the proximal femur. Bone 50, 824–829.
Koivumäki, J.E., Thevenot, J., Pulkkinen, P., Kuhn, V., Link, T.M., Eckstein, F., Jämsä, T., 2012b. Cortical bone finite element models in the estimation of experimentally measured failure loads in the proximal femur. Bone 51, 737–740.
Langton, C.M., Pisharody, S., Keyak, J.H., 2009. Comparison of 3D finite element analysis derived stiffness and BMD to determine the failure load of the excised proximal femur. Med. Eng. Phys. 31, 668–672.
Lenaerts, L., Van Lenthe, G.H., 2009. Multi-level patient-specific modelling of the proximal femur. A promising tool to quantify the effect of osteoporosis treatment. Philos. Trans. R. Soc. A Math. Phys. Eng. Sci. 367, 2079–2093.
Leslie, W.D., Lix, L.M., Johansson, H., Oden, A., McCloskey, E., Kanis, J.A., 2010. Independent clinical validation of a Canadian FRAX® tool: fracture prediction and model calibration. J. Bone Miner. Res. 25 (11), 2350–2358.
Lewiecki, E.M., Compston, J.E., Miller, P.D., et al., 2011a. Official Positions for FRAX((R)) Bone Mineral Density and FRAX((R)) Simplification From Joint Official Positions Development Conference of the International Society for Clinical Densitometry and International Osteoporosis Foundation on FRAX((R)). J. Clin. Densitom. 14, 226–236.
Lewiecki, E.M., Compston, J.E., Miller, P.D., et al., 2011b. FRAX((R)) Bone Mineral Density Task Force of the 2010 Joint International Society for Clinical Densitometry & International Osteoporosis Foundation Position Development Conference. J. Clin. Densitom. 14, 223–225.
Lotz, J.C., Cheal, E.J., Hayes, W.C., 1991. Fracture prediction for the proximal femur using finite element models. I. Linear analysis. *Transactions of the ASME*. J. Biomech. Eng. 113 (4), 353–360.
Luo, Y., Ferdous, Z., Leslie, W.D., 2011. A preliminary dual-energy X-ray absorptiometry-based finite element model for assessing osteoporotic hip fracture risk. J. Eng. Med. 225, 1188–1195.
Luo, Y., Ferdous, Z., Leslie, W.D., 2013. Precision study of DXA-based patient-specific finite element modeling for assessing hip fracture risk. Int. J. Numer. Methods Biomed. Eng. 29 (5), 615–629.
MacNeil, J.A., Boyd, S.K., 2008. Bone strength at the distal radius can be estimated from high resolution peripheral quantitative computed tomography and the finite element method. Bone 42, 1203–1213.
Marshall, D., Johnell, O., Wedel, H., 1996. Meta-analysis of how well measures of bone mineral density predict occurrence of osteoporotic fractures. BMJ 312, 1254–1259.
Melton III, L.J., 1993. Hip fractures: a worldwide problem today and tomorrow. Bone 14 (Supplement 1), 1–8.
Michelotti, J., Clark, J., 1999. Femoral neck length and hip fracture risk. J. Bone Miner. Res. 14, 1714–1720.
Michelson, J.D., Myers, A., Jinnah, R., Cox, Q., Van Natta, M., 1995. Epidemiology of hip fractures among the elderly: risk factors for fracture type. Clin. Orthop. Relat. Res. 311, 129–135.
Nankaku, M., Kanzaki, H., Tsuboyama, T., Nakamura, T., 2005. Evaluation of hip fracture risk in relation to fall direction. Osteoporos. Int. 16 (11), 1315–1320.
Naylor, K.E., McCloskey, E.V., Eastell, R., Yang, L., 2013. Use of DXA-based finite element analysis of the proximal femur in a longitudinal study of hip fracture. 28, 1014–1021.
Orwoll, E.S., Marshall, L.M., Nielson, C.M., et al., 2009. Finite element analysis of the proximal femur and hip fracture risk in older men. J. Bone Miner. Res. 24, 475–483.
Papadimitropoulos, E.A., Coyte, P.C., Josse, R.G., Greenwood, C.E., 1997. Current and projected rates of hip fracture in Canada. CMAJ 157, 1357–1363.
Papaioannou, A., Wiktorowicz, M.E., Adachi, J.D., Goeree, R., Papadimitropoulos, M., Weaver, B., 2000. Mortality, independence in living, and re-fracture, one year following hip fracture in Canadians. J. Soc. Obstet. Gynaecol. Can. 22, 591–597.
Qian, J.-G., Song, Y.-W., Tang, X., Zhang, S., 2009. Examination of femoral-neck structure using finite element model and bone mineral density using dual-energy X-ray absorptiometry. Clin. Biomech. 24, 47–52.
FRAX®: WHO Fracture Risk Assessment Tool. http://www.shef.ac.uk/FRAX/. World Health Organization Collaborating Centre for Metabolic Bone Diseases, University of Sheffield, UK.
Rhee, Y., Hur, J.H., Won, Y.Y., et al., 2009. Assessment of bone quality using finite element analysis based upon micro-CT images. Clin. Orthop. Surg. 1, 40–47.
Silva, M.J., 2007. Biomechanics of osteoporotic fractures. Injury 38 (Suppl. 3), S69–S76.
Stone, K.L., Seeley, D.G., Lui, L.Y., et al., 2003. BMD at multiple sites and risk of fracture of multiple types: long-term results from the Study of Osteoporotic Fractures. J. Bone Miner. Res. 18, 1947–1954.
Testi, D., Viceconti, M., Baruffaldi, F., Cappello, A., 1999. Risk of fracture in elderly patients: a new predictive index based on bone mineral density and finite element analysis. Comput. Methods Prog. Biomed. 60, 23–33.
Tosteson, A.N.A., Gottlieb, D.J., Radley, D., Fisher, E.S., Melton, L.J.I., 2007. Excess mortality following hip fracture: the role of underlying health status. Osteoporos. Int. 1463–1472.
Trabelsi, N., Yosibash, Z., Wutte, C., et al., 2011. Patient-specific finite element analysis of the human femur—a double-blinded biomechanical validation. J. Biomech. 44, 1666–1672.
Trémollieres, F.A., Pouillès, J.M., Drewniak, N., Laparra, J., Ribot, C.A., Dargent-Molina, P., 2010. Fracture risk prediction using BMD and clinical risk factors in early postmenopausal women: sensitivity of the WHO FRAX tool. J. Bone Miner. Res. 25, 1002–1009.
Wiktorowicz, M.E., Goeree, R., Papaioannou, A., Adachi, J.D., Papadimitropoulos, E., 2001. Economic implications of hip fracture: health service use, institutional care and cost in Canada. Osteoporos. Int. 12, 271–278.